

OPEN ACCESS

EDITED BY Du Yuan, Changsha University of Science and Technology, China

REVIEWED BY
Yao Meng,
Sichuan University, China
Bakusele Kabane,
Durban University of Technology, South Africa

*CORRESPONDENCE
Tingjun Wu,

☑ tingjun.wu@hotmail.com
Nosang V. Myung,
☑ nmyung@nd.edu

RECEIVED 25 May 2025 ACCEPTED 25 July 2025 PUBLISHED 01 September 2025 CORRECTED 11 September 2025

CITATION

Wu T, Kim J, Choa Y-H and Myung NV (2025) Electrodeposition of nanocrystalline Fe_XCo_{1-X} thin films from choline chloride—urea deep eutectic solvents.

Front. Chem. 13:1635084. doi: 10.3389/fchem.2025.1635084

COPYRIGHT

© 2025 Wu, Kim, Choa and Myung. This is an open-access article distributed under the terms of the Creative Commons Attribution License (CC BY). The use, distribution or reproduction in other forums is permitted, provided the original author(s) and the copyright owner(s) are credited and that the original publication in this journal is cited, in accordance with accepted academic practice. No use, distribution or reproduction is permitted which does not comply with these terms.

Electrodeposition of nanocrystalline Fe_XCo_{1-X} thin films from choline chloride—urea deep eutectic solvents

Tingjun Wu¹*, Jiwon Kim², Yong-Ho Choa³ and Nosang V. Myung^{4,5}*

¹Xiamen Institute of Rare Earth Materials, Xiamen, Fujian, China, ²Center for Advanced Materials, Institute for Advanced Engineering, Yongin, Gyeonggi, Republic of Korea, ³Department of Materials Science and Chemical Engineering, Hanyang University, Ansan-si, Republic of Korea, ⁴Department of Chemical and Biomolecular Engineering, University of Notre Dame, Notre Dame, IN, United States, ⁵Department of Chemistry and Biochemistry, University of Notre Dame, Notre Dame, IN, United States

 Fe_xCo_{1-x} thin films were electrodeposited from a choline–urea deep eutectic solvent (DES) containing Fe^{3+} and Co^{2+} ions under ambient conditions. Anomalous co-deposition was observed, with Fe preferentially depositing over Co. With higher cathodic potential, the film's morphology shifted from smooth to nodular. X-ray diffraction (XRD) analysis showed iron oxide impurities at lower overpotential and temperatures (e.g., <-0.9 V at 70 °C), while impurity-free, nanocrystalline $Co_{50}Fe_{50}$ films had formed at higher temperatures (e.g., 130 °C). The films exhibited a body-centered cubic (BCC) structure with (110) preferred orientation and grain sizes of 30 nm–40 nm.

KEYWORDS

deep eutectic solvent, choline chloride, urea, electrodeposition, CoFe, soft magnetic materials

Introduction

Soft magnetic materials, which can easily be magnetized or demagnetized, have many applications from magnetic storage media to recording head (Ikeda et al., 2010; Okada et al., 2002; Okada et al., 2004; Parkin et al., 2008; Sato et al., 2012) to spintronic-based magnetic racetrack memories (Arnold et al., 2006; Judy and Muller, 1996; Lenz, 1990), inductors (Popovic et al., 1996), actuators (Bozorth, 1951), sensors (Liu et al., 2004; Scheunert et al., 2016), and microelectromechanical systems (MEMS) and nanoelectromechanical systems (NEMS) (Cooper et al., 2005; Kim et al., 2014; Osaka, 2000; Romankiw, 1997). The most desirable soft magnetic properties are high saturation magnetization ($M_{\rm s}$), high permeability, low coercivity ($H_{\rm c}$), and low core loss. Thus, most soft magnetic materials are derived from the iron group metals (i.e., Ni, Fe, and Co).

 Fe_XCo_{1-X} binary alloys are important soft magnetic materials with excellent magnetic properties, including relatively low coercivity (~2 Oe), low hysteresis loss, high electric permeability, high saturation magnetization (e.g., M_s of 2.4 T for $Co_{50}Fe_{50}$) (Shao et al., 2007; Shao et al., 2010), and relatively high electrical resistance (Andricacos and Robertson, 1998; Brankovic, 2012; Burkert et al., 2004; Cooper et al., 2005; Ehrfeld, 2003; Ghemes et al., 2017; Ghemes et al., 2017; Kohn et al., 2001; Sahari et al., 2006; Turgut et al., 1998; Zhan et al., 2002). Especially, nanocrystalline Fe_XCo_{1-X} alloys are highly desirable materials for high-temperature applications, such as magnetic bearings for high-speed motor, flywheels

(Yu et al., 2000), and gas turbine engines (Fingers et al., 1999; Giri et al., 2000; Kortus et al., 2002; Shang C. H. et al., 2000; Shang C.-H. et al., 2000; Turgut et al., 2000).

Although many synthesis methods are available for the preparation of Fe_XCo_{1-X} films (Ashar, 1997; Shao et al., 2003), electrodeposition is an important processing technology because of its low capital/equipment and operating cost, high yield, low energy consumption, fast deposition rates, ability to handle complex geometries, high scalability, and capability (Dini, 1993; Wu et al., 2016; Wu et al., 2017). In addition, the material properties (e.g., morphology, composition, crystallinity, and crystal structures) can be readily tailored by controlling the electrodeposition parameters (Bai and Hu, 2003; Kockar et al., 2010; Lallemand et al., 2004).

Electrodeposition of Fe_XCo_{1-X} has been investigated by many groups. Most of Fe_XCo_{1-X} binary alloys were electrodeposited in acidic aqueous baths, with Fe2+ and Co2+ being used as precursors in aqueous media. In these works, solution parameters such as pH (Brankovic et al., 2006) and additives (Brankovic et al., 2008) and electrodeposition parameters such as deposition potential (Brankovic et al., 2009) were adjusted to control the film morphology and microstructures, which resulted in different magnetic properties. With respect to acidic baths, several major challenges need to be overcome to achieve high saturation magnetization (M_s ≥2.4 T). First, Fe³⁺ ions are always present in the aqueous solution because of the oxidation of Fe²⁺ either by the dissolved oxygen from the air or by the anode surface during the Fe_XCo_{1-X} thin-film electrodeposition (Elhalawaty et al., 2011; Elhalawaty et al., 2012; Lide, 2005; Mehrizi et al., 2012; Zhang and Ivey, 2004). Moreover, electrodeposition of Fe_XCo_{1-X} films in an aqueous solution is a process where the dramatic hydrogen gas evolution reaction occurs in parallel, leading to the increase in local pH at the electrode/solution interface and precipitation of insoluble metal hydroxides, especially Fe(OH)₃ because of its low solubility (Mehrizi et al., 2012), in the Fe_XCo_{1-X} films (Brankovic et al., 2008; Zhang and Ivey, 2004). Precipitation of non-magnetic metal hydroxide particles would decrease the saturation magnetization of the aqueous solution and shorten the bath life (Brankovic et al., 2008; Osaka et al., 2003). It was reported that a critical concentration of Fe³⁺ >1.2 mM in solution results in a dramatic decrease in the M_s value of the CoFe alloy by ~44% (George et al., 2013; Tabakovic et al., 2006). In addition, the oxygen content in a CoFe film should remain lower than 1%-3% to reach a high saturation magnetization (Brankovic et al., 2008; Elhalawaty et al., 2011; Gao et al., 2006; Riemer et al., 2009). As a consequence, the incorporation of Fe(OH)₃ in the deposit is the major obstacle in obtaining Fe_xCo_{1-x} films and nanostructures with high saturation magnetization (Shao et al., 2007) and low coercivity (Yue et al., 2009). The accumulation of Fe³⁺ ions in solution is normally prevented by continuous chemical reduction (e.g., L-ascorbic acid) of Fe3+ ions to Fe2+ ions (Abd El-Halim and Fawzy, 1993; Almasi Kashi et al., 2010; Brener, 1994; Elbaile et al., 2012; Esmaeily et al., 2013; Huang et al., 2010; Ji et al., 2014; Kim et al., 2012; Ramazani et al., 2011; Schlesinger and Paunovic, 2011; Viqueira et al., 2015; Yang et al., 2010). The second challenge in the electrodeposition of Fe_XCo_{1-X} films in an aqueous solution is that they undergo anomalous co-deposition, in which the less noble metal (i.e., Fe) deposits preferentially (Osaka et al., 1999a; Popov et al., 1993; Schlesinger and Paunovic, 2000). Additionally, additives were normally used in aqueous solution to improve the brightness and crystal structure, achieve smaller grain size, and reduce the residual stresses in the deposit (Brankovic et al., 2007; Osaka et al., 1999a; Osaka et al., 2003). However, additive molecules or molecular fragments can be found in the deposits as well (Brankovic et al., 2005; Brankovic et al., 2007; Edwards, 1962; Frankel et al., 1993; George et al., 2008). For example, the existence of sulfur in the magnetic deposit from saccharin as an additive occurs either via saccharin adsorption–electroreduction or via its physical incorporation during the deposit growth (Osaka et al., 1999b; Osaka et al., 2003). The significant presence of the interstitials, such as boron, sulfur, metal sulfides, or S-containing organic molecules, can cause a deterioration in the alloy's magnetic performance and corrosion resistance (Osaka, 2000; Osaka et al., 1998; Smith et al., 2014).

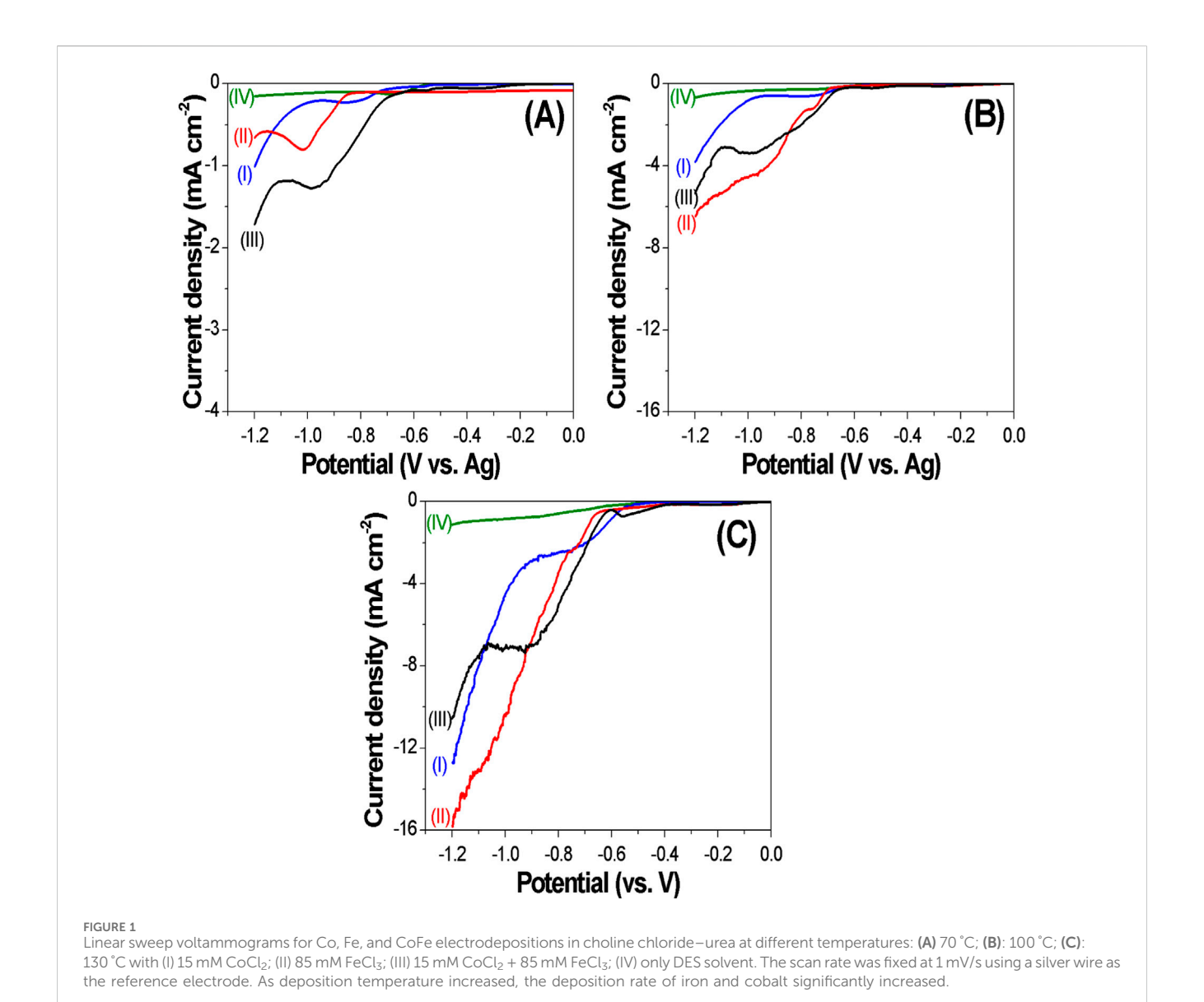
Deep eutectic solvents (DESs), a class of ionic solutions closely related to ionic liquids but contain organic components (e.g., urea, amide, and acid), have emerged as new electrolytes for electrodeposition because of their relatively low vapor pressure; high tolerance of humidity; good thermo-stability; high solubility of metal precursors including metal salts, metal oxides, and metal hydroxides (Abbott et al., 2003; Binnemans et al., 2015; Brankovic et al., 2006; Brankovic et al., 2008); and greater deposition potential windows compared to aqueous electrolytes (Brankovic et al., 2009). Other advantages of DESs compared to aqueous bath have been highlighted by many authors (Bockris and Conway, 1975; Dulal et al., 2007).

Miller et al. (2017) investigated electrodeposition of iron thin films from choline chloride–ethylene glycol, with FeCl₃ as the iron precursor. They observed that the iron complex is strongly dependent on the chloride-to-iron ratio. For example, when the ratio is greater than 4, [FeCl₄]⁻ and [FeCl₄]⁻² are dominant iron complexes, whereas ethylene glycol forms a complex with iron when the ratio is less than 4 (Endres et al., 2017). Yanai et al. reported the galvanostatic deposition of Fe_XCo_{1-X} alloys at a fixed current density of 67 mA/cm² from choline chloride–ethylene glycol electrolytes with FeCl₂ and CoCl₂ as metal precursors at 100 °C (Yanai et al., 2015). They demonstrated the ability to for electrodeposition of smooth Fe_XCo_{1-X} thin films at high current efficiency (>90%). The magnetic saturation of the deposits was in good agreement with the Slater–Pauling curve.

 $Fe_{X}Co_{1-X}$ thin films have been systematically electrodeposited in the choline chloride–urea DES with $FeCl_{3}$ and $CoCl_{2}$ as precursors. Unlike other reported data, various electroanalytical methods including linear sweep voltammograms (LSVs) and chronoamperograms (CAs) were utilized to investigate the electrodeposition mechanism. Furthermore, $Fe_{X}Co_{1-X}$ films were synthesized using a potentiostatic method under varying potentials and temperatures, and their effects on the composition, morphology, crystal structures, and magnetic properties were systematically investigated.

Experimental procedure

The DES was prepared by mixing the choline chloride and urea (1:2 ratio) at 80 °C until completely liquefied. Additionally, anhydrous cobalt chloride (CoCl₂) and anhydrous iron chloride (FeCl₃) were added and dissolved in the DES. The concentrations of FeCl₃ and CoCl₂ were fixed at 85 and 15 mM, respectively.

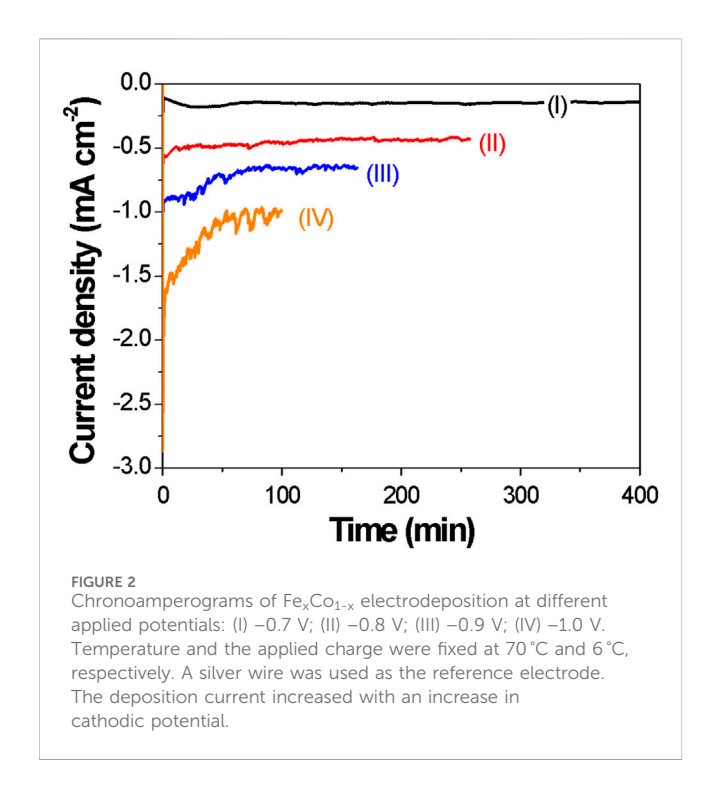


Electrodeposition experiments were performed in a conventional three-electrode cell using a platinum-coated silicon wafer as the working electrode. Platinum-coated titanium stripes and silver were used as the counter and reference electrodes, respectively. The total charge was fixed at 6 C. Linear sweep voltammetry (LSV) was conducted to investigate the electrodeposition mechanisms of $Fe_{\rm X}Co_{1-{\rm X}}$ with a fixed scan rate of 1 mV/s. The effect of the applied potential and temperature was investigated by varying the applied potential from -0.7 to -1.0 V and the temperature from $70\,^{\circ}{\rm C}$ to $130\,^{\circ}{\rm C}$.

The morphology, composition, and crystal orientation of tellurium films were investigated by scanning electron microscopy (SEM, TESCAN VEGA), energy-dispersive spectroscopy (EDX, Ametek), and X-ray diffraction (XRD, PANalytical Empyrean) with 0.026° increments. The average grain size was determined using the Scherrer equation. The current efficiency (CE) was determined by measuring the mass of the electrodeposited ${\rm Fe_{X}Co_{1-X}}$ films divided by the mass calculated from the charge based on CAs.

Results and discussion

Figure 1 shows the temperature-dependent linear sweep voltammograms of electrolytes containing CoCl₂ (I), FeCl₃ (II), and CoCl2 and FeCl3 (III) and that without metal salts (IV) from 70 °C to 130 °C. In the absence of metal salts, the cathodic current density was relatively low, which indicates that there was a minor side reaction due to the decomposition of urea, where the onset potential of DES decomposition shifted positively from -0.56, -0.50, and -0.44 V as the temperature increased from 70 °C, 100 °C, and 130 °C, respectively. In the presence of metal salts, the current density significantly increased with increasing temperature at a fixed potential. For example, the electrolyte containing only CoCl2 as metal ions showed a reduction peak at the applied potential of approximately -0.8 V, which represents the electrochemical reduction of Co²⁺ to Co(s) (blue curve). The electrolyte only containing FeCl₃ showed a cathodic peak at the applied potential of approximately -1.0V, which represents the electrochemical reduction of Fe⁺³ to Fe(s). As expected, the electrolyte containing



both $CoCl_2$ and $FeCl_3$ shows two cathodic peaks. Additionally, at a fixed applied potential of -0.8 V, the reduction current density of Co increased from -0.2 to -0.61 to -2.5 mA cm⁻², the current density of Fe increased from -0.1 to -1.4 to -3.4 mA cm⁻², and the current density of Fe_XCo_{1-X} increased from -0.55 to -1.9 to 5.0 mA cm⁻² as the temperature increased from 70 °C to 100 °C to 130 °C.

Figure 1A shows that when the applied potential changed from -0.7 to -0.8 V, the average current density of Co increased from -0.07 to -0.20 mA cm⁻², but when the applied potential further varied to -0.9 and -1.0 V, the current density of Co deposition remained at approximately 0.22 mA cm⁻². As shown in the LSV curve I in Figure 1A, in the applied potential range of -0.8 to -1.0 V, the electrodeposition of Co reached a limiting current, where the electrochemical reduction reaction altered from kinetic control to mass transfer control. For iron electrodeposition at 70 °C, the current density continuously increases when the applied potential becomes more negative (Figure 1A; curve II). This is probably the reason why when the applied potential became more negative, the Fe content increased. In the acidic baths, anomalous co-deposition is observed, and Fe, the less noble metal, is deposited preferentially (Dulal et al., 2007). In DES, the same phenomenon was observed. For example, at an applied potential of -0.8 V at 70 °C, according to the LSV data (Figure 1A), the current density of Co and Fe deposition was -0.20 and -0.11 mA cm⁻², respectively. However, the Fe content of the Fe_xCo_{1-X} film deposited at −0.8 V and 70 °C is 56%, which means that the less noble metal (i.e., Fe) was preferentially electrodeposited.

It is well-known that the magnetic properties of Fe_XCo_{1-X} films are greatly affected by their compositions and microstructures (Dulal et al., 2007; Natter and Hempelmann, 1996; Wu et al., 2016); thus, a reliable control of the composition and microstructure is essential. The effect of the applied potential on electrodeposition of Fe_XCo_{1-X} thin films was investigated under potentiostatic conditions at 70 °C. As shown in the CAs (Figure 2), current transients are relatively constant at the low applied potential of -0.7 and -0.8 V. However, at a higher applied potential (e.g., -0.9 and -1.0 V), the current transients started to fluctuate.

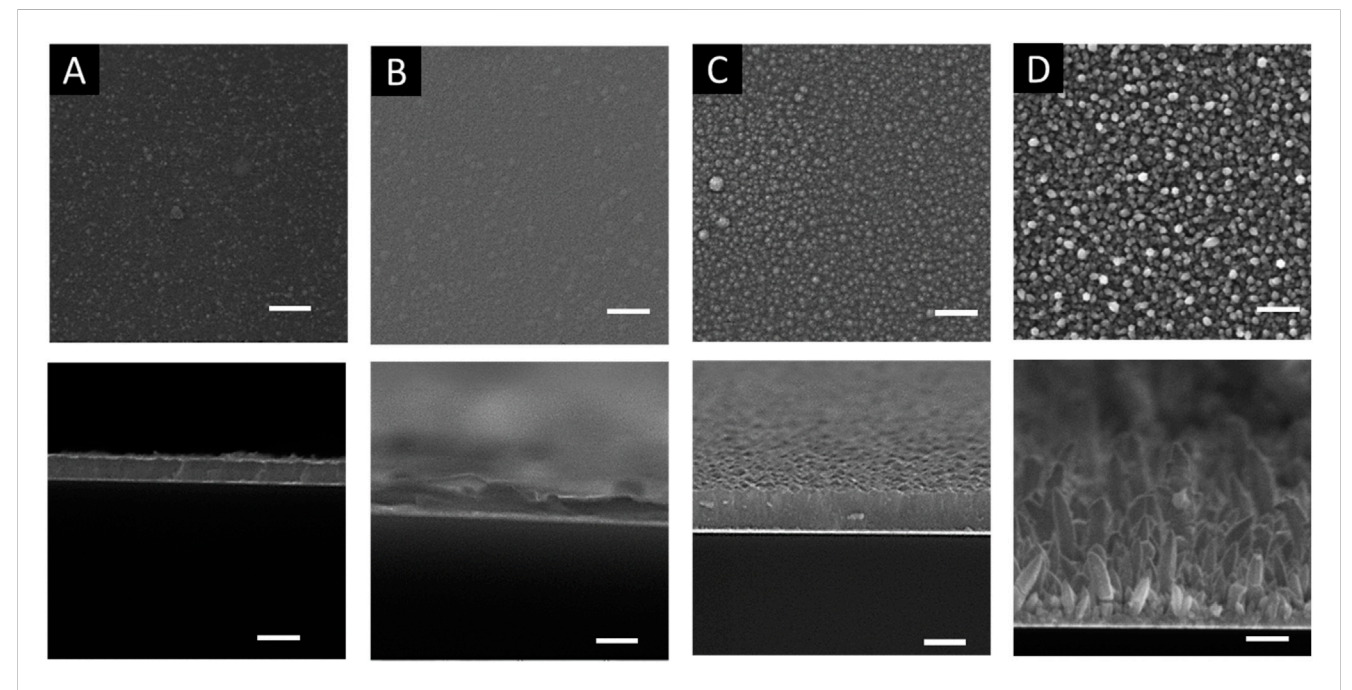


FIGURE 3 SEM images of Fe_xCo_{1-x} electrodeposited at different applied potentials: (A) -0.7 V; (B) -0.8 V; (C) -0.9 V; (D) -1.0 V with 15 mM $CoCl_2 + 85$ mM $FeCl_3$ at the temperature of 70 °C. The top row images are the cross-sectional view, and the bottom row images are the top view. The length bars represent 2 microns. The morphology significantly changed with applied potential from smooth to nodular morphology.

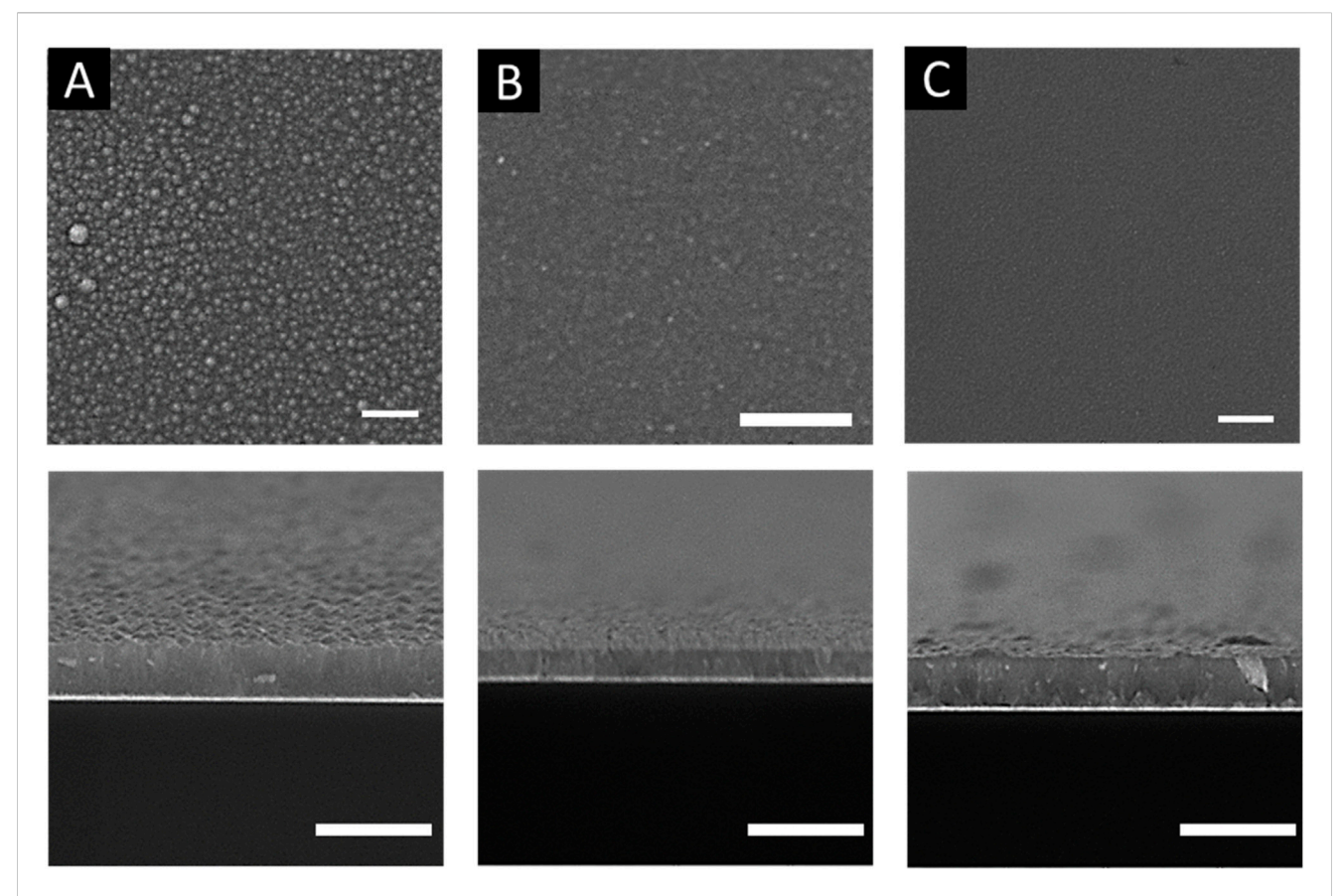


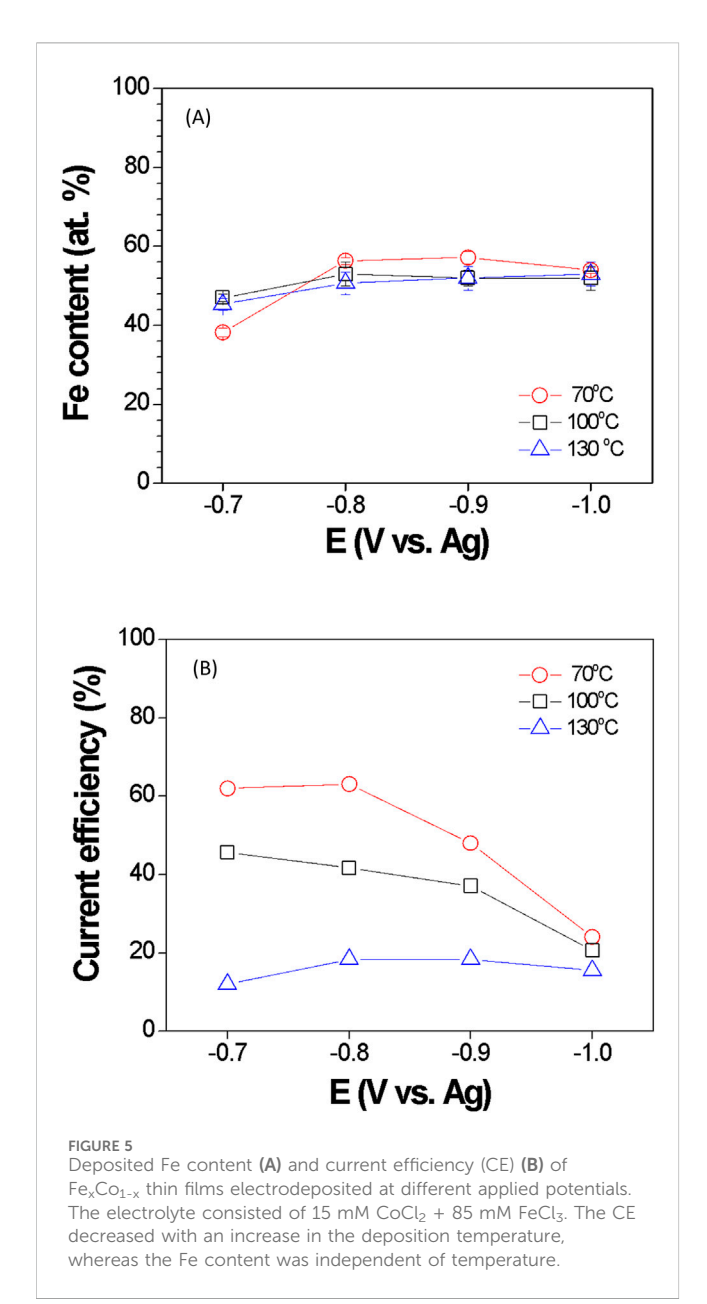
FIGURE 4 SEM images of Fe_xCo_{1-x} electrodeposited at different temperatures: (A) 70 °C; (B) 100 °C; (C) 130 °C with 15 mM $CoCl_2 + 85$ mM $FeCl_3$ at the applied potential of -0.9 V. The top row images are the cross-sectional view, and the bottom row images are the top view. The length bars represent 2 microns. As the deposition temperature increased, the film's morphology became more smoother.

Figure 3 shows the top (top row) and cross-sectional (bottom row) images of electrodeposition of Fe_XCo_{1-X} thin films. At an applied potential of -0.7 to -0.9 V, the cross-sectional images (Figure 3 bottom row) showed that the electrodeposited films were compact with nodular surface morphology (Figure 3 top row). The nodular size increases with increasing applied potential. At an applied potential of -1.0 V, the morphology changed to a nanorod array with the average diameter of approximately 400 nm. According to the LSV curve III in Figure 1A, when the applied potential was more negative than -0.96 V, the deposition current reached a limiting current, indicating that mass transfer of metal ions limits the electrochemical reaction. Consequently, with the applied potential of -1.0 V, the morphology of electrodeposited Fe_XCo_{1-X} was no longer a compact film. Fe_xCo_{1-X} deposited in DES at −1.0 V showed a nanorod array instead of a porous or dendritic morphology, which are typically observed in electrodeposits under mass transfer limits (Dulal et al., 2007).

The electrodeposition temperature was found to significantly affect the morphology and magnetic properties of electrodeposited films (Dulal et al., 2007; Natter and Hempelmann, 1996). The effect of temperature on the electrodeposition of Fe_XCo_{1-X} was investigated at the applied potential of -0.9~V by varying the temperature from 70~C to 130~C. The CA curves at different temperatures (i.e., 70~C, 100~C, and 130~C) are shown in

Figure 3. According to the figure, the current density increased with increasing reaction temperature, and the CA curves fluctuated at higher temperatures. The effects of the reaction temperature on the morphology of Fe_XCo_{1-X} films are presented by SEM images in Figure 4. As shown in the figure, the surface morphology of the films was smoother when the temperature was increased from 70 °C to 130 °C.

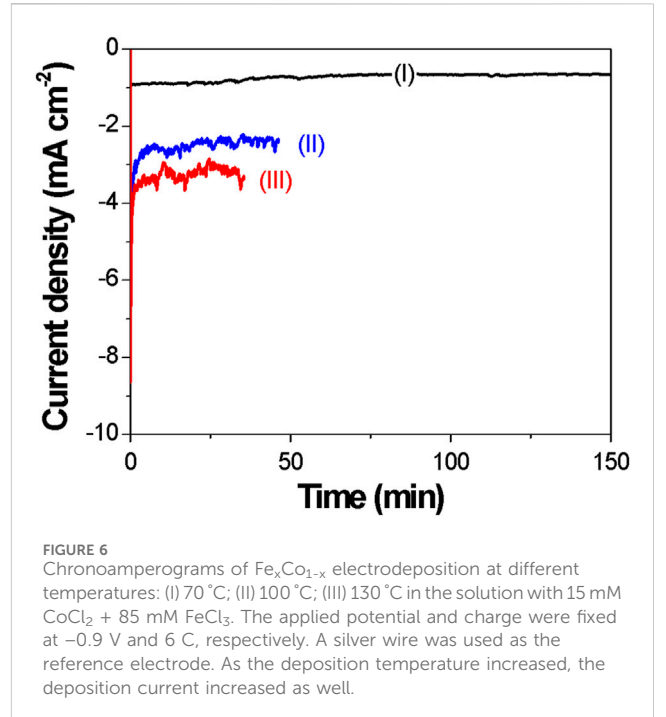
The effects of the applied potential and temperature on Fe content are shown in Figure 5. At 70 °C, the Fe content increased from 38 at. % to 56 at. %, when the applied potential was varied from -0.7 to -0.8 V; when the applied potential further increased to -0.9 V, the Fe content increased slightly to 57 at. %; however, at the applied potential of -1.0 V, the Fe content decreased to 54 at. %. At 100 °C, the Fe content increased from 47 at. % to 53 at. % when the applied potential was changed from -0.7 to -0.8 V; however, the Fe content remained at 52 at. %, when the applied potential was changed from -0.9 to -1.0 V. At 130 °C, the Fe content increased significantly from 45 to 51 at. %, when the applied potential was changed from -0.7 to -0.8 V; however, when the applied potential varied from -0.9 to -1.0 V, the Fe content increased slightly from 52 at. % to 53 at. %, respectively. In general, the increase in Fe content as a function of overpotential is consistent with LSV data, in which, at higher overpotential, the current density of Fe deposition is higher, while the current density of Co electrodeposition remains approximately constant (Figure 1). Unlike the deposited Fe content,



the current efficiency significantly depended on the operating temperature and applied potential, where it decreased with the increase in temperature and cathodic potential (Figure 6B).

It is a well-known phenomenon that the less noble metal (Fe) deposits preferentially over the more noble metal (Co) in an aqueous solution, primarily due to complexation and adsorption effects (Gonçalves et al., 2023; Zhou et al., 2012). Ferric ions can form complex ions with chloride, with the most common species in the aqueous solution being [FeCl₄]. At high chloride concentrations and under acidic conditions, the formation of [FeCl₄] is favored. This can shift the redox equilibrium between ferrous and ferric ions to the left, as shown in Equation 1, effectively increasing the electrode potential of the Fe³⁺/Fe²⁺ couple. Additionally, the formation of such complexes further influences the redox potential.

$$Fe^{3+} + e^{-} \rightleftharpoons Fe^{2+}$$
. (1)

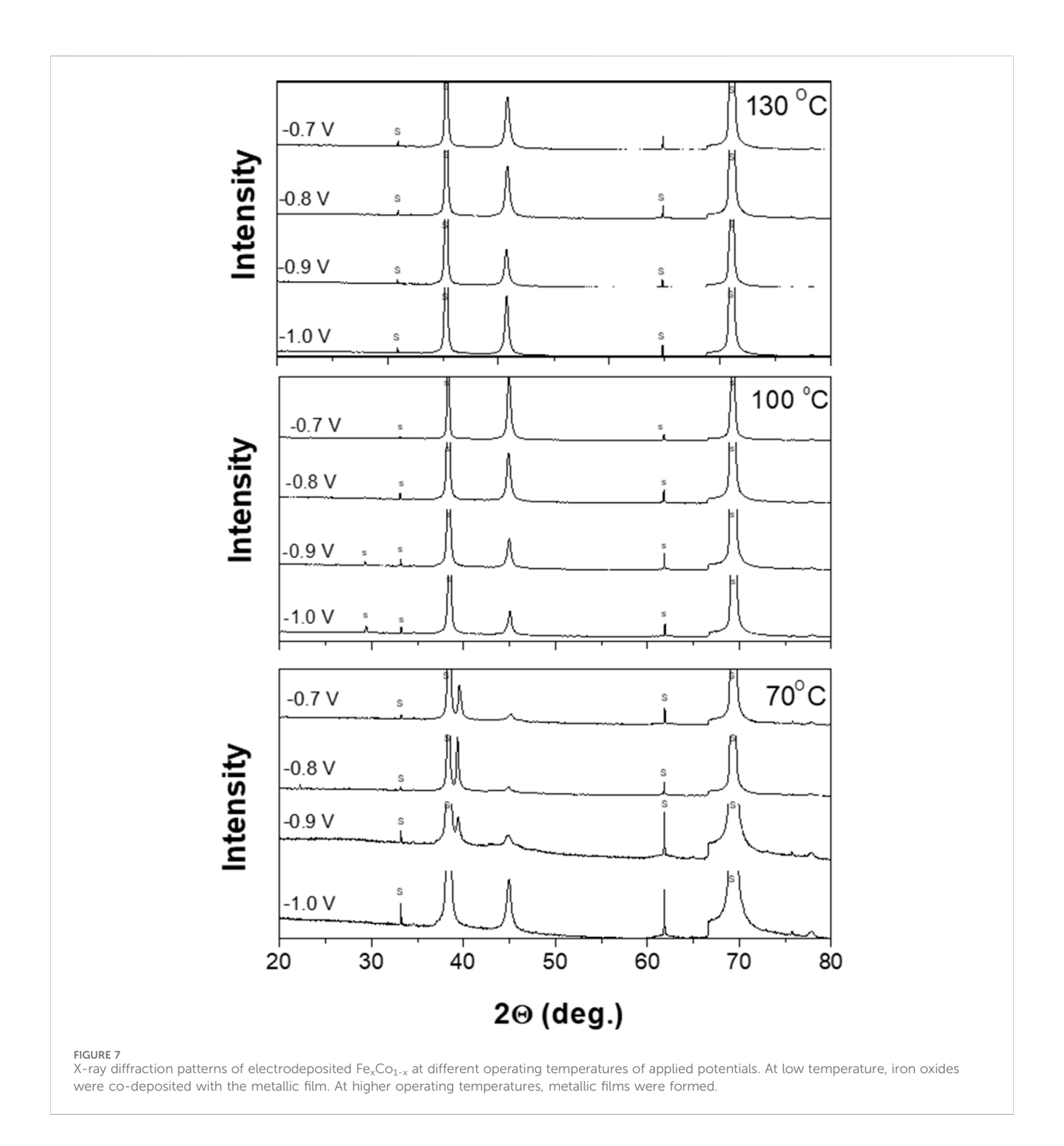


Similarly, cobalt(II) ions can also form complexes with chloride ions, particularly $[CoCl_4]^{2-}$. The formation of $[CoCl_4]^{2-}$ also contributes to a shift in the redox potential.

Anomalous electrodeposition in DESs has also been reported in the literature. The underlying causes are similar to those observed in aqueous solutions, where anomalous deposition is associated with ion complexation and reaction kinetics (Doneux et al., 2024). Additionally, mass transport limitations because of the high viscosity of DESs can restrict ion diffusion, thereby favoring the deposition of metal ions with faster electron transfer kinetics (Bernasconi et al., 2017).

Figure 7 shows the XRD patterns of electrodeposited Fe_XCo_{1-X} films as a function of the applied potential at a fixed temperature of 70 °C. Electrodeposited films from -0.7 to -0.9 V showed (110) a peak from body-centered cubic (BCC) FeCo and a (200) peak from α -Fe₂O₃. However, at an applied potential of -1.0 V, the deposit only showed the BCC (110) peak. During the electrodeposition process, the Fe3+ ions will be absorbed to the electrode first, followed by electrochemical reduction at the electrode surface (Dulal et al., 2007). At a low applied potential, the electrochemical reduction rate might not be sufficient enough to reduce all the absorbed Fe³⁺ ions; therefore, a certain amount of Fe3+ ions remained in the electrodeposited Fe_XCo_{1-X}, which was confirmed by the α-Fe₂O₃ peak. At an applied potential of -1.0 V, the reaction became mass transfer control, and the electrochemical reaction was high enough to reduce all of the absorbed Fe3+ ions on the electrode. This is probably the reason why there is no Fe₂O₃ peak in the XRD data at an applied potential of -1.0 V.

As the deposition temperatures increased to $100\,^{\circ}\text{C}$ and $130\,^{\circ}\text{C}$, the XRD patterns only showed a (110) peak. This is probably because the high temperature results in a higher electrochemical



reaction rate, which makes it fast enough to reduce all the $\mathrm{Fe^{3+}}$ ions absorbed on the electrode.

The average grain size of the electrodeposited Fe_XCo_{1-X} films was estimated by the Scherrer equation. At the temperature of 70 °C, the average grain size of Fe_XCo_{1-X} was ~35 nm at the applied potentials of -0.7 and -0.8 V; when the applied potential became more negative to -0.9 and -1.0 V, the average grain size reduced to ~30 nm. At 100 °C, the average grain size increased from 31 to 37 nm when the applied potential was increased

from -0.7 to -0.8 V; however, when the applied potential further increased from -0.9 to -1.0 V, the average grain size maintained at approximately 37 nm. At the temperature of 130 °C, the average grain size of $\rm Fe_{\rm X}Co_{1-\rm X}$ was approximately 35 nm when the applied potential was -0.7 and -0.8 V, and it increased to 39 nm when the applied potential was changed to -1.0 V. In summary, the overall variation of $\rm Fe_{\rm X}Co_{1-\rm X}$ grain size as a function of the applied potential and temperature is small, which is from $\sim\!\!29$ to 39 nm.

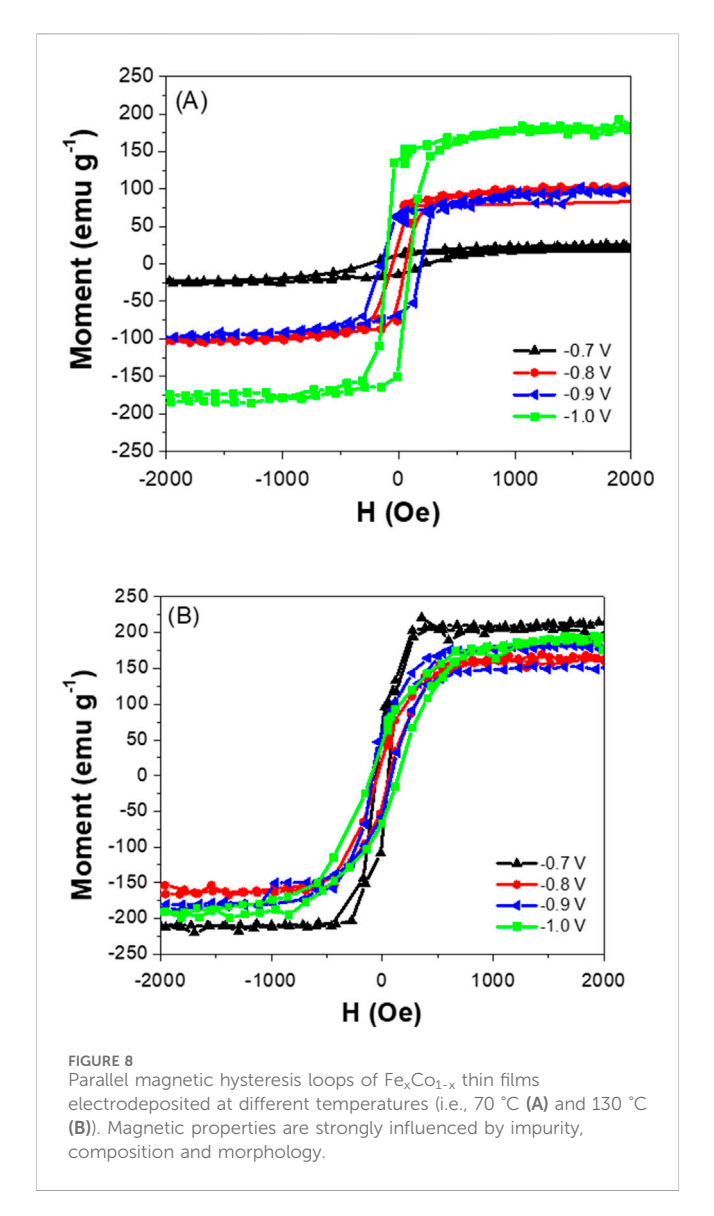
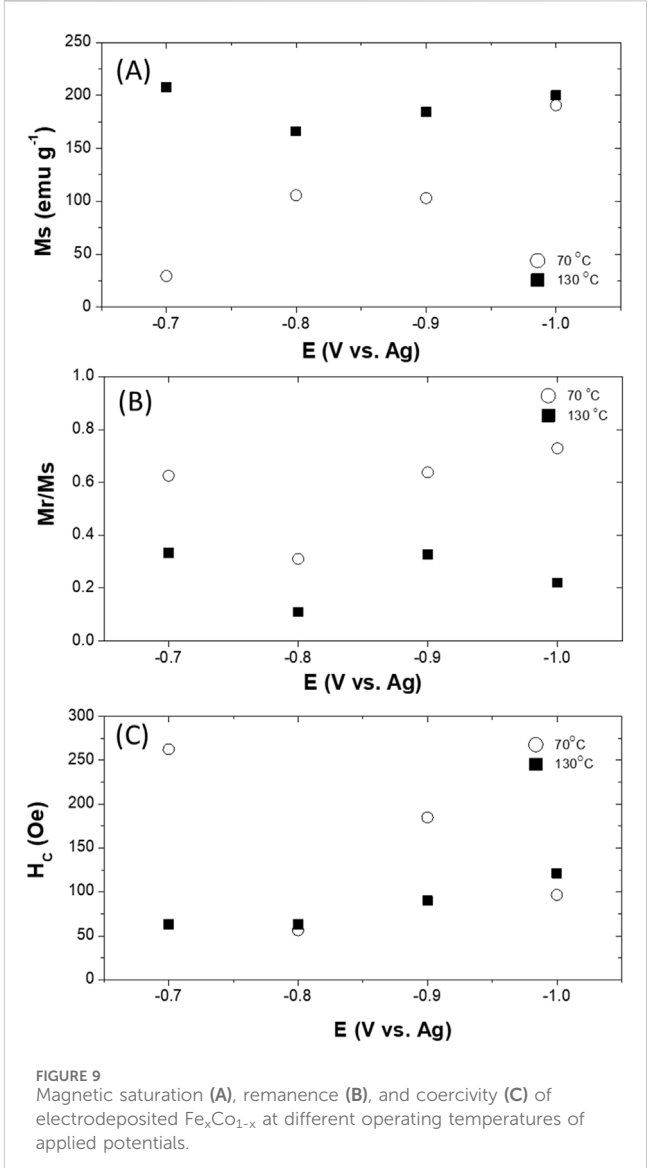


Figure 8 shows the parallel magnetic hysteresis loops of Fe_xCo_{1-x} thin films electrodeposited at different temperatures (i.e., 70 °C and 130 °C). As expected, magnetic saturation (M_s) showed a monotonic increase with increasing cathodic potential at 70 °C, whereas M_s was less dependent on the applied potentials (Figure 9A). The lower M_s may be attributed to the presence of α-Fe₂O₃ in the deposit. At high deposition temperature, only metallic Fe_xCo_{1-X} were electrodeposited with similar composition, resulting in similar M_s . As shown in Figures 9B, C, composite electrodeposited films showed greater squareness (M_r/M_s) and higher coercivity due to the co-existence of α-Fe₂O₃ in the deposit.

Supplementary Table S1 compares the magnetic properties of electrodeposited FeCo thin films from both aqueous and DES baths. As shown in the table, the intrinsic magnetic saturation (M_s) strongly depends on the film composition, regardless of the bath type. However, extrinsic coercivity (H_c) is highly influenced by both the composition and deposition conditions, including the nature of the electrolyte solution (i.e., aqueous or DES).



Conclusion

Fe_xCo_{1-x} thin films were electrodeposited in a DES solution using Fe³⁺ and Co²⁺ as precursors without reducing agents or other additives. The films had a smooth compact morphology when the applied potential was at the kinetic controlled range, while the morphology shifted to a nanorod array when the deposition was carried out under mass transfer control. The composition of Fe_XCo_{1-X} films and current efficiency can be altered by varying the applied potential and deposition temperature. Generally, the Fe content increases first and then reaches a plateau when the applied potential varies from -0.7 to -1.0 V. The increase in Fe content as a function of overpotential may be caused by a higher Fe deposition rate at high overpotential, which is consistent with LSV data. Most of the Fe_XCo_{1-X} electrodeposits from the DES show a bodycentered cubic crystal structure with the preferred orientation of (110). All electrodeposited Fe_XCo_{1-X} films had small grains ranging from 29 to 39 nm. At low temperatures and low cathodic potentials, co-deposition of iron oxide was observed. At higher

cathodic potentials and elevated operating temperatures, the codeposition of iron oxide was minimized or completely suppressed. The magnetic properties were strongly influenced by the presence of iron oxide.

Data availability statement

The original contributions presented in the study are included in the article/Supplementary Material, further inquiries can be directed to the corresponding authors.

Author contributions

TW: Writing – original draft, Data curation. JK: Writing – review and editing, investigation, Conceptualization. Y-HC: Conceptualization, Data curation, Funding acquisition, Writing – review and editing, NM: Writing – review and editing, Funding acquisition, Conceptualization, Project administration.

Funding

The author(s) declare that financial support was received for the research and/or publication of this article. JK likes to acknowledges the funding suppport by the Industrial Innovation Infrastructure Construction Project (RS-2024-00435498) and Demand-Driven Next-Generation Researchers Industrial Innovation Technology Development Program (RS-2025-16063993) funded by Ministry of Trade, Industry and Energy (MOTIE, Korea), Republic of Korea.

References

Abbott, A. P., Capper, G., Davies, D. L., Rasheed, R. K., and Tambyrajah, V. (2003). Novel solvent properties of choline chloride/urea mixtures. *Chem. Commun.* (1), 70–71. doi:10.1039/b210714g

Abd El-Halim, A. M., and Fawzy, M. H. (1993). Acid - electroplating of Co-Fe alloys from aqueous sulphate baths. *Trans. IMF* 71 (4), 125–128.

Almasi Kashi, M., Ramazani, A., Es'haghi, F., Ghanbari, S., and Esmaeily, A. (2010). Acid - microstructures and magnetic properties of as-deposited and annealed $\text{Fe}_x\text{Co}_{1-x}$ alloy nanowire arrays embedded in anodic alumina templates. *Phys. B Condens. Matter* 405 (12), 2620–2624. doi:10.1016/j.physb.2010.03.012

Andricacos, P. C., and Robertson, N. (1998). Future directions in electroplated materials for thin-film recording heads. *IBM J. Res. Dev.* 42 (5), 671–680. doi:10. 1147/rd.425.0671

Arnold, D. P., Das, S., Cros, F., Zana, I., Allen, M., and Lang, J. (2006). Magnetic induction machines integrated into bulk-micromachined silicon. *J. Microelectromechanical Syst.* 15 (2), 406–414. doi:10.1109/jmems.2006.873951

Ashar, K. G. (1997). Magnetic disk drive technology. New York: IEEE.

Bai, A., and Hu, C.-C. (2003). Iron-cobalt and iron-cobalt-nickel nanowires deposited by means of cyclic voltammetry and pulse-reverse electroplating. *Electrochem. Commun.* 5 (1), 78–82. doi:10.1016/s1388-2481(02)00540-4

Bernasconi, R., Panzeri, G., Accogli, A., Liberale, F., Nobili, L., Magagnin, L., et al. (2017). *Electrodeposition from deep eutectic solvents*. IntechOpen.

Binnemans, K., Jones, P. T., Müller, T., and Yurramendi, L. (2015). Rare-earths and the balance problem: how to deal with changing markets? *Chem. Rev.* 115 (10), 4263–4307.

Bockris, J. O., and Conway, B. E. (1975). Modern aspects of electrochemistry. Springer US.

Bozorth, R. M. (1951). Ferromagnetism, 194. New York: D.Van. Nostrand Co. Inc.

Conflict of interest

The authors declare that the research was conducted in the absence of any commercial or financial relationships that could be construed as a potential conflict of interest.

Correction note

This article has been corrected with minor changes. These changes do not impact the scientific content of the article.

Generative AI statement

The author(s) declare that no Generative AI was used in the creation of this manuscript.

Publisher's note

All claims expressed in this article are solely those of the authors and do not necessarily represent those of their affiliated organizations, or those of the publisher, the editors and the reviewers. Any product that may be evaluated in this article, or claim that may be made by its manufacturer, is not guaranteed or endorsed by the publisher.

Supplementary material

The Supplementary Material for this article can be found online at: https://www.frontiersin.org/articles/10.3389/fchem.2025.1635084/full#supplementary-material

Brankovic, S. R. (2012). Saccharin effect on properties of 2.4 T CoFe films. Electrochimica Acta 84, 139–144. doi:10.1016/j.electacta.2012.07.061

Brankovic, S. R., Vasiljevic, N., Klemmer, T. J., and Johns, E. C. (2005). Influence of additive adsorption on properties of pulse deposited CoFeNi alloys. *J. Electrochem. Soc.* 152 (4), C196–C202. doi:10.1149/1.1864352

Brankovic, S. R., XiaoMin Yang, Klemmer, T., and Seigler, M. (2006). Pulse electrodeposition of 2.4 T $Co_{37}Fe_{63}$ alloys at nanoscale for magnetic recording application. *IEEE Trans. Magnetics* 42 (2), 132–139. doi:10.1109/tmag.2005.861778

Brankovic, S. R., Haislmaier, R., and Vasiljevic, N. (2007). Physical incorporation of saccharin molecules into electrodeposited soft high magnetic moment CoFe alloys. *Electrochem. Solid-State Lett.* 10 (6), D67. doi:10.1149/1.2722038

Brankovic, S. R., Bae, S. E., and Litvinov, D. (2008). Acid - the effect of Fe³⁺ on magnetic moment of electrodeposited CoFe alloys-Experimental study and analytical model. *Electrochimica Acta* 53 (20), 5934–5940. doi:10.1016/j. electacta.2008.03.071

Brankovic, S. R., George, J., Bae, S., and Litvinov, D. (2009). Critical parameters of solution design for electrodeposition of 2.4 T CoFe alloys. *ECS Trans.* 16 (45), 75–87. doi:10.1149/1.3140012

Brener, A. (1994). Electrodeposition of alloys. New York: Academic Press. Inc.

Burkert, T., Nordström, L., Eriksson, O., and Heinonen, O. (2004). Giant magnetic anisotropy in tetragonal FeCo alloys. *Phys. Rev. Lett.* 93 (2), 027203. doi:10.1103/physrevlett.93.027203

Cooper, E. I., Bonhote, C., Heidmann, J., Hsu, Y., Kern, P., Lam, J. W., et al. (2005). Recent developments in high-moment electroplated materials for recording heads. *IBM J. Res. Dev.* 49 (1), 103–126. doi:10.1147/rd.491.0103

Dini, J. W. (1993). Electrodeposition - the materials science of coating and substrates. Westwood, NJ: Noyes Publications.

- Doneux, T., Sorgho, A., Soma, F., Rayée, Q., and Bougouma, M. (2024). Electrodeposition in deep eutectic solvents: the "obvious", the "unexpected" and the "wonders". *Molecules* 29, 3439. doi:10.3390/molecules29143439
- Dulal, S. M. S. I., Yun, H. J., Shin, C. B., and Kim, C. K. (2007). Electrodeposition of CoWP film: III. Effect of pH and temperature. *Electrochimica Acta* 53 (2), 934–943. doi:10.1016/j.electacta.2007.08.006
- Edwards, J. (1962). Radiotracer study of addition agent behaviour: 3—incorporation of sulphur in nickel deposited from solutions containing $_{\rm p}$ -toluenesulphonamide and saccharin. Trans. Inst. Metal Finish. 39 (52), 52–55. doi:10.1080/00202967.1962. 11879192
- Ehrfeld, W. (2003). Electrochemistry and microsystems. Electrochimica Acta 48 (20), 2857–2868. doi:10.1016/s0013-4686(03)00350-5
- Elbaile, L., Crespo, R. D., Vega, V., and García, J. A. (2012). Magnetostatic interaction in Fe-Co nanowires. *J. Nanomater.* 2012, 1–6. doi:10.1155/2012/198453
- Elhalawaty, S., Carpenter, R. W., George, J., and Brankovic, S. R. (2011). Oxygen incorporation into electrodeposited CoFe films: consequences for structure and magnetic properties. *J. Electrochem. Soc.* 158 (11), D641. doi:10.1149/2.011111jes
- Elhalawaty, S., Carpenter, R. W., George, J., and Brankovic, S. R. (2012). Nanostructure and oxide phase distribution in Co36-40Fe64-60 electrodeposited films for magnetic field sensors. *J. Appl. Phys.* 111 (7), 07A330. doi:10.1063/1.3677931
- Endres, F., Abbott, A., and MacFarlane, D. R. (2017). Electrodeposition from ionic liquids. 2nd ed. (Wiley VCH).
- Esmaeily, A. S., Venkatesan, M., Razavian, A. S., and Coey, J. M. D. (2013). Diameter-modulated ferromagnetic CoFe nanowires. *J. Appl. Phys.* 113 (17), 17A327. doi:10.1063/1.4794722
- Fingers, R. T., Coate, J. E., and Dowling, N. E. (1999). Creep deformation of a soft magnetic iron-cobalt alloy. J. Appl. Phys. 85 (8), 6037-6039. doi:10.1063/1.369074
- Frankel, G. S., Brusic, V., Schad, R., and Chang, J. W. (1993). Pitting corrosion of electroplated permalloy films. *Corros. Sci.* 35 (1), 63–71. doi:10.1016/0010-938x(93) 90134-3
- Gao, J.-H., Zhan, Q. F., He, W., Sun, D. L., and Cheng, Z. H. (2006). Thermally activated magnetization reversal process of self-assembled Fe55Co45 nanowire arrays. *J. Magnetism Magnetic Mater.* 305 (2), 365–371. doi:10.1016/j.jmmm.2006.01.028
- George, J., Rantschler, J., Bae, S. E., Litvinov, D., and Brankovic, S. R. (2008). Sulfur and saccharin incorporation into electrodeposited CoFe alloys: consequences for magnetic and corrosion properties. *J. Electrochem. Soc.* 155 (9), D589–D594. doi:10.1149/1.2948377
- George, J., Elhalawaty, S., Mardinly, A. J., Carpenter, R., Litvinov, D., and Brankovic, S. R. (2013). Oxide/hydroxide incorporation into electrodeposited CoFe alloys—consequences for magnetic softness. *Electrochimica Acta* 110, 411–417. doi:10.1016/j.electacta.2013.06.097
- Ghemes, A., Dragos-Pinzaru, O., Chiriac, H., Lupu, N., Grigoras, M., Shore, D., et al. (2017). Controlled electrodeposition and magnetic properties of Co35Fe65 nanowires with high saturation magnetization. *J. Electrochem. Soc.* 164 (2), D13–D22. doi:10.1149/2041702jee
- Giri, A. K., Chowdary, K., Humfeld, K., and Majetich, S. (2000). AC magnetic properties of FeCo nanocomposites. *IEEE Trans. Magnetics* 36 (5), 3026–3028. doi:10. 1109/20.908665
- Gonçalves, S., Andrade, V., Sousa, C. T., Araújo, J. P., Belo, J. H., and Apolinário, A. (2023). Tunable iron–cobalt thin films grown by electrodeposition. *Magnetochemistry* 9, 161. doi:10.3390/magnetochemistry9070161
- Huang, C., Wang, P., Guan, W., Yang, S., Gao, L., Wang, L., et al. (2010). Improved microstructure and magnetic properties of iron-cobalt nanowire via an ac electrodeposition with a multistep voltage. *Mater. Lett.* 64 (22), 2465–2467. doi:10. 1016/j.matlet.2010.08.026
- Ikeda, S., Miura, K., Yamamoto, H., Mizunuma, K., Gan, H. D., Endo, M., et al. (2010). A perpendicular-anisotropy CoFeB–MgO magnetic tunnel junction. *Nat. Mater.* 9, 721–724. doi:10.1038/nmat2804
- Ji, R., Cao, C., Chen, Z., and Yao, R. (2014). Synthesis of crystalline CoFex nanowire arrays through high voltage pulsed electrochemical deposition. *J. Magnetism Magnetic Mater.* 363, 95–102. doi:10.1016/j.jmmm.2014.03.054
- Judy, J. W., and Muller, R. S. (1996). Magnetic micro actuation of torsional polysilicon structures. *Sensors Actuators A Phys.* 53 (1), 392–397. doi:10.1016/0924-4247(96) 01138-7
- Kim, B. G., Yoon, S. J., Jeon, I. T., Kim, K. H., Wu, J. H., and Kim, Y. K. (2012). Dimensional dependence of magnetic properties in arrays of CoFe/Au barcode nanowire. *IEEE Trans. Magnetics* 48 (11), 3929–3932. doi:10.1109/tmag.2012. 2202101
- Kim, K., Xu, X., Guo, J., and Fan, D. L. (2014). Ultrahigh-speed rotating nanoelectromechanical system devices assembled from nanoscale building blocks. *Nat. Commun.* 5, 3632. doi:10.1038/ncomms4632
- Kockar, H., Alper, M., Sahin, T., and Karaagac, O. (2010). Role of electrolyte pH on structural and magnetic properties of Co–Fe films. *J. Magnetism Magnetic Mater.* 322 (9), 1095–1097. doi:10.1016/j.jmmm.2009.10.058

- Kohn, A., Eizenberg, M., Shacham-Diamand, Y., and Sverdlov, Y. (2001). Characterization of electroless deposited Co(W,P) thin films for encapsulation of copper metallization. *Mater. Sci. Eng. A* 302 (1), 18–25. doi:10.1016/s0921-5093(00) 01348-4
- Kortus, J., Baruah, T., Pederson, M. R., Ashman, C., and Khanna, S. N. (2002). Magnetic moment and anisotropy in FenCom clusters. *Appl. Phys. Lett.* 80 (22), 4193–4195. doi:10.1063/1.1482793
- Lallemand, F., Comte, D., Ricq, L., Renaux, P., Pagetti, J., Dieppedale, C., et al. (2004). Effects of organic additives on electroplated soft magnetic CoFeCr films. *Appl. Surf. Sci.* 225 (1), 59–71. doi:10.1016/j.apsusc.2003.09.033
- Lenz, J. E. (1990). A review of magnetic sensors. *Proc. IEEE* 78 (6), 973–989. doi:10. 1109/5.56910
- Lide, D. R. (2005). CRC handbook of chemistry and physics.
- Liu, Y., Zhang, J., Yu, L., Jia, G., Zhang, Y., Wang, X., et al. (2004). Frequency and magnetic properties in the range of 10 kHz to 100 MHz for nanocrystal Fe–Co alloy. *Curr. Appl. Phys.* 4 (5), 455–460. doi:10.1016/j.cap.2004.02.001
- Mehrizi, S., Heydarzadeh Sohi, M., Shafahian, E., and Khangholi, A. A. (2012). Studies of electrical resistivity and magnetic properties of nanocrystalline CoFeCu thin films electrodeposited from citrate-added baths. *J. Mater. Sci. Mater. Electron.* 23 (6), 1174–1181. doi:10.1007/s10854-011-0568-6
- Miller, M. A., Wainright, J. S., and Savinell, R. F. (2017). Iron electrodeposition in a deep eutectic solvent for flow batteries. *J. Electrochem. Soc.* 164 (4), A796–A803. doi:10. 1149/2.1141704jes
- Natter, H., and Hempelmann, R. (1996). Nanocrystalline copper by pulsed electrodeposition: the effects of organic additives, bath temperature, and pH. *J. Phys. Chem.* 100 (50), 19525–19532. doi:10.1021/jp9617837
- Okada, T., Kawato, Y., Haginoya, C., Nunokawa, I., Etoh, K., and Fuyama, M. (2002). Fabrication process for a trapezoidal main pole for single-pole-type heads. *IEEE Trans. Magnetics* 38 (5), 2249–2252. doi:10.1109/tmag.2002.802781
- Okada, T., Kimura, H., Nunokawa, I., Yoshida, N., Etoh, K., and Fuyama, M. (2004). Fabricating narrow and trapezoidal main poles for single-pole-type heads. *IEEE Trans. Magnetics* 40 (4), 2329–2331. doi:10.1109/tmag.2004.830215
- Osaka, T. (2000). Electrodeposition of highly functional thin films for magnetic recording devices of the next century. *Electrochimica Acta* 45 (20), 3311–3321. doi:10. 1016/s0013-4686(00)00407-2
- Osaka, T., Takai, M., Hayashi, K., Ohashi, K., Saito, M., and Yamada, K. (1998). A soft magnetic CoNiFe film with high saturation magnetic flux density and low coercivity. *Nature* 392, 796–798. doi:10.1038/33888
- Osaka, T., Sawaguchi, T., Mizutani, F., Yokoshima, T., Takai, M., and Okinaka, Y. (1999a). Effects of saccharin and thiourea on sulfur inclusion and coercivity of electroplated soft magnetic CoNiFe film. *J. Electrochem. Soc.* 146 (9), 3295–3299. doi:10.1149/1.1392470
- Osaka, T., Takai, M., Sogawa, Y., Momma, T., Ohashi, K., Saito, M., et al. (1999b). Influence of crystalline structure and sulfur inclusion on corrosion properties of electrodeposited CoNiFe soft magnetic films. *J. Electrochem. Soc.* 146 (6), 2092–2096. doi:10.1149/1.1391896
- Osaka, T., Yokoshima, T., Shiga, D., Imai, K., and Takashima, K. (2003). A high moment CoFe soft magnetic thin film prepared by electrodeposition. *Electrochem. Solid-State Lett.* 6 (4), C53. doi:10.1149/1.1554291
- Parkin, S. S. P., Hayashi, M., and Thomas, L. (2008). Magnetic domain-wall racetrack memory. Science 320 (5873), 190–194. doi:10.1126/science.1145799
- Popov, B. N., Yin, K. M., and White, R. E. (1993). Galvanostatic pulse and pulse reverse plating of nickel-iron alloys from electrolytes containing organic compounds on a rotating disk electrode. *J. Electrochem. Soc.* 140 (5), 1321–1330. doi:10.1149/1.2220978
- Popovic, R. S., Flanagan, J. A., and Besse, P. A. (1996). The future of magnetic sensors. Sensors Actuators A Phys. 56 (1), 39–55. doi:10.1016/0924-4247(96)01285-x
- Ramazani, A., Almasi Kashi, M., Kabiri, S., and Zanguri, M. (2011). Acid the influence of asymmetric electrodeposition voltage on the microstructure and magnetic properties of Fe_xCo_{1-x} nanowire arrays. *J. Cryst. Growth* 327 (1), 78–83. doi:10.1016/j. jcrysgro.2011.05.011
- Riemer, S., Gong, J., Sun, M., and Tabakovic, I. (2009). Influence of solution pH and concentration of saccharin on electrodeposition and properties of 2.4 T CoFe alloys. *J. Electrochem. Soc.* 156 (10), D439. doi:10.1149/1.3194773
- Romankiw, L. T. (1997). A path: from electroplating through lithographic masks in electronics to LIGA in MEMS. *Electrochimica Acta* 42 (20), 2985–3005. doi:10.1016/s0013-4686(97)00146-1
- Sahari, A., Azizi, A., Schmerber, G., Abes, M., Bucher, J., and Dinia, A. (2006). Electrochemical nucleation and growth of Co and CoFe alloys on Pt/Si substrates. *Catal. Today* 113 (3-4), 257–262. doi:10.1016/j.cattod.2005.11.075
- Sato, H., Yamanouchi, M., Ikeda, S., Fukami, S., Matsukura, F., and Ohno, H. (2012). Perpendicular-anisotropy CoFeB-MgO magnetic tunnel junctions with a MgO/CoFeB/Ta/CoFeB/MgO recording structure. *Appl. Phys. Lett.* 101 (2), 022414. doi:10.1063/1.4736727

Scheunert, G., Heinonen, O., Hardeman, R., Lapicki, A., Gubbins, M., and Bowman, R. M. (2016). A review of high magnetic moment thin films for microscale and nanotechnology applications. *Appl. Phys. Rev.* 3 (1), 011301. doi:10.1063/1.4941311

Schlesinger, M., and Paunovic, M. (2000). Modern electroplating. New York: John Wiley and Sons.

Schlesinger, M., and Paunovic, M. (2011). Modern electroplating. John Wiley and Sons. Inc.

Shang, C. H., Weihs, T. P., Cammarata, R. C., Ji, Y., and Chien, C. L. (2000a). Anisotropy in magnetic and mechanical properties in textured Hiperco® FeCoV alloys. *J. Appl. Phys.* 87 (9), 6508–6510. doi:10.1063/1.372753

Shang, C.-H., Cammarata, R. C., Weihs, T. P., and Chien, C. L. (2000b). Microstructure and Hall–petch behavior of Fe–Co-based Hiperco® alloys. *J. Mater. Res.* 15 (4), 835–837. doi:10.1557/jmr.2000.0118

Shao, I., Vereecken, P. M., Chien, C. L., Cammarata, R. C., and Searson, P. C. (2003). Electrochemical deposition of FeCo and FeCoV alloys. *J. Electrochem. Soc.* 150 (3), C184. doi:10.1149/1.1553789

Shao, I., Chen, M. W., Cammarata, R. C., Searson, P. C., and Prokes, S. M. (2007). Acid - deposition and characterization of Fe_{0.55}Co_{0.45} nanowires. *J. Electrochem. Soc.* 154 (11), D572. doi:10.1149/1.2772201

Shao, I., Romankiw, L. T., and Bonhote, C. (2010). Stress in electrodeposited CoFe alloy films. *J. Cryst. Growth* 312 (8), 1262–1266. doi:10.1016/j.jcrysgro.2009. 11.061

Smith, E. L., Abbott, A. P., and Ryder, K. S. (2014). Deep eutectic solvents (DESs) and their applications. *Chem. Rev.* 114 (21), 11060–11082. doi:10.1021/cr300162p

Tabakovic, I., Riemer, S., Tabakovic, K., Sun, M., and Kief, M. (2006). Mechanism of saccharin transformation to metal sulfides and effect of inclusions on corrosion susceptibility of electroplated CoFe magnetic films. *J. Electrochem. Soc.* 153 (8), C586. doi:10.1149/1.2207821

Turgut, Z., Scott, J. H., Huang, M. Q., Majetich, S. A., and McHenry, M. E. (1998). Magnetic properties and ordering in C-coated Fe_xCo_{1-x} alloy nanocrystals. *J. Appl. Phys.* 83 (11), 6468–6470. doi:10.1063/1.367922

Turgut, Z., Fingers, R., Piehler, H., and McHenry, M. (2000). Microstructural and magnetic observations of compacted FeCoV nanoparticles. *IEEE Trans. Magnetics* 36 (5), 3024–3025. doi:10.1109/20.908664

Viqueira, M. S., Bajales, N., Urreta, S. E., and Bercoff, P. G. (2015). Acid magnetization mechanisms in ordered arrays of polycrystalline Fe_{100-x} Co_x nanowires. *J. Appl. Phys.* 117 (20), 204302. doi:10.1063/1.4921701

Wu, T., Lee, H.-K., and Myung, N. V. (2016). Electrodeposition of dense lead telluride thick films in alkaline solutions. *J. Electrochem. Soc.* 163 (14), D801–D808. doi:10.1149/2.0631614ies

Wu, T., Zhang, M., Lee, K. H., Lee, C. M., Lee, H. K., Choa, Y., et al. (2017). Electrodeposition of compact tellurium thick films from alkaline baths. *J. Electrochem. Soc.* 164 (2), D82–D87. doi:10.1149/2.1191702jes

Yanai, T., Shiraishi, K., Watanabe, Y., Ohgai, T., Nakano, M., Suzuki, K., et al. (2015). Magnetic Fe-Co films electroplated in a deep-eutectic-solvent-based plating bath. J. Appl. Phys. 117 (17). doi:10.1063/1.4918782

Yang, W., Cui, C., Sun, J., and Wang, B. (2010). Acid - fabrication and magnetic properties of Fe $_3$ Co $_7$ alloy nanowire arrays. *J. Mater. Sci.* 45 (6), 1523–1527. doi:10.1007/s10853-009-4116-1

Yu, R. H., Basu, S., Ren, L., Zhang, Y., Parvizi-Majidi, A., Unruh, K., et al. (2000). High temperature soft magnetic materials: FeCo alloys and composites. *IEEE Trans. Magnetics* 36 (5), 3388–3393. doi:10.1109/20.908809

Yue, G. H., Wang, X., Wang, L., Chang, P., Wen, R., Chen, Y., et al. (2009). Acid structure and magnetic properties of $Fe_{1-x}Co_x$ nanowires in self-assembled arrays. Electrochimica Acta 54 (26), 6543–6547. doi:10.1016/j.electacta.2009.06.037

Zhan, Q., Chen, Z., Xue, D., Li, F., Kunkel, H., Zhou, X., et al. (2002). Structure and magnetic properties of Fe-Co nanowires in self-assembled arrays. *Phys. Rev. B* 66, 134436. doi:10.1103/physrevb.66.134436

Zhang, Y., and Ivey, D. G. (2004). Electroplating of nanocrystalline CoFeNi soft magnetic thin films from a stable citrate-based bath. *Chem. Mater.* 16 (7), 1189–1194. doi:10.1021/cm035306u

Zhou, D., Zhou, M., Zhu, M., Yang, X., and Yue, M. (2012). Electrodeposition and magnetic properties of FeCo alloy films. *J. Appl. Phys.* 111 (7), 07A319. doi:10.1063/13675063